

Supporting Information

Transfer of Transition-Metal Dichalcogenide Circuits onto Arbitrary Substrates for Flexible Device Applications

Hyebin Lee‡, *Kookjin Lee*‡, *Yanghee Kim*, *Hyunjin Ji*, *Junhee Choi*, *Minsik Kim*, *Jae-Pyoung Ahn**, and *Gyu-Tae Kim**

H. B. Lee, K. J. Lee, Prof. G. -T. Kim
School of Electrical Engineering, Korea University, Seoul 02841, Republic of Korea

Y. H. Kim, Dr. J. -P. Ahn
Advanced Analysis Center, Korea Institute of Science and Technology, Seoul 02792,
Republic of Korea

Dr. H. J. Ji
Department of Energy Science, Sungkyunkwan University, Suwon 16419, Republic of Korea

Dr. J. H. Choi
Surface Technology Division, Korea Institute of Materials Science (KIMS), 797
Changwondaero, Sungsan-Gu, Changwon, Gyeongnam 51508, Republic of Korea

M. S. Kim
School of Mechanical Engineering, Korea University, Seoul 02841, Republic of Korea

*E-mail : gtkim@korea.ac.kr(G.-T.K.), jpahn@kist.re.kr(J.-P.A.)

‡These authors contributed equally.

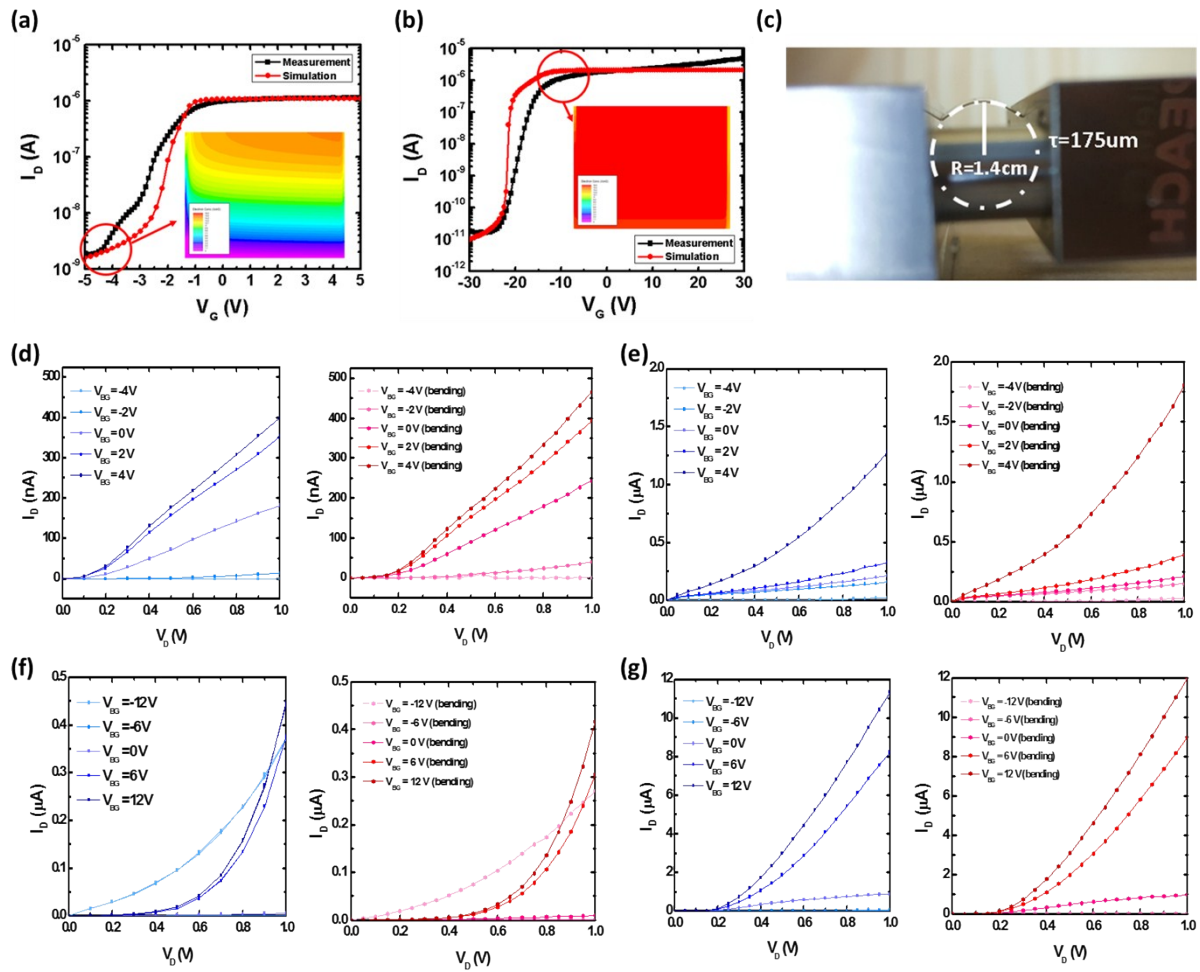


Figure S1. Transfer characteristic curves (I_D - V_G) of MoS₂ FETs on (a) Al₂O₃/ITO/PET and (b) SiO₂/Si in a log scale with measurement (black) and simulation by TCAD (red). The insets refer to the carrier concentration of each channel. (c) The photograph of the flexible sample at a bending radius of 1.4 cm on the experimental bend. Output characteristic (I_D - V_D) of (d) MoS₂ FETs on Al₂O₃/ITO/PET before bending and after 200 times bending test, and (e) WSe₂ FETs on Al₂O₃/ITO/PET at before bending and after bending at different gate voltages. Output characteristics (I_D - V_D) of (f) MoS₂ FETs on Al₂O₃/ITO/PET with Al₂O₃ passivation before bending and after 200 times bending test, and (g) WSe₂ FETs on Al₂O₃/ITO/PET at before bending and after bending at different gate voltages.

Figure S1 shows transfer characteristic curves of MoS₂ FETs on (a) Al₂O₃/ITO/PET and (b) SiO₂/Si in a log scale with measurement (black) and simulation by TCAD (red). The insets

refer to the carrier concentration of each channel. The simulation proceeds to SILVACO TCAD and the channel thickness is set to 60 nm. Using a 90 nm thick SiO₂ as a gate dielectric, the depletion region of the channel is not formed, whereas using 30 nm of Al₂O₃, an electron concentration gradient of the channel occurs. We can calculate the bending of the flexible substrate with radius of $R = 1.4$ cm, and the induced strain in our devices is $\varepsilon = \tau/R$, where $\tau = 175$ μm is the thickness of PET. Figure S1 (d) – (e) show output characteristics of transferred MoS₂ devices, measured at drain voltages from 0 V to 1 V and gate voltages from -4 V to 4 V. Figure S1 (f) – (g) show output characteristics of transferred WSe₂ devices, measured at drain voltages from 0 V to 1 V and gate voltages from -12 V to 12 V.

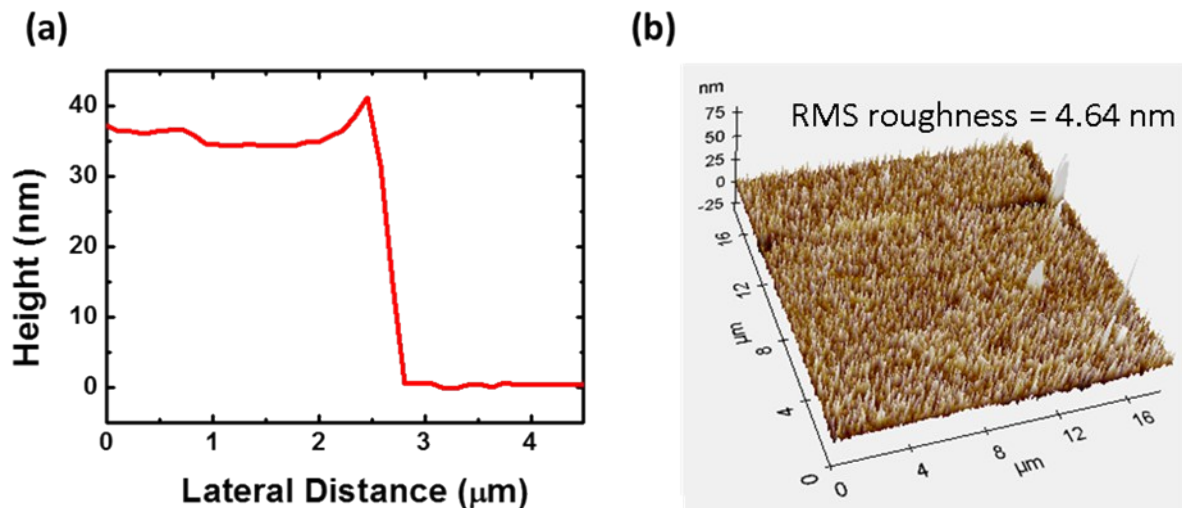


Figure S2. (a) The height profile of an Al₂O₃ film on ITO and channels (b) AFM topography of Al₂O₃ film on ITO

The thickness of the thin Al₂O₃ film is measured by AFM, and both Al₂O₃ layers of passivation and gate dielectric are estimated to be 38 nm in thickness (see Figure S2 (a)). AFM topography of Al₂O₃ film on ITO is referred in Figure S2 (b) and RMS roughness is calculated by 4.64 nm. Since the value of RMS roughness is larger than that of other thin films, the surface condition is poor.

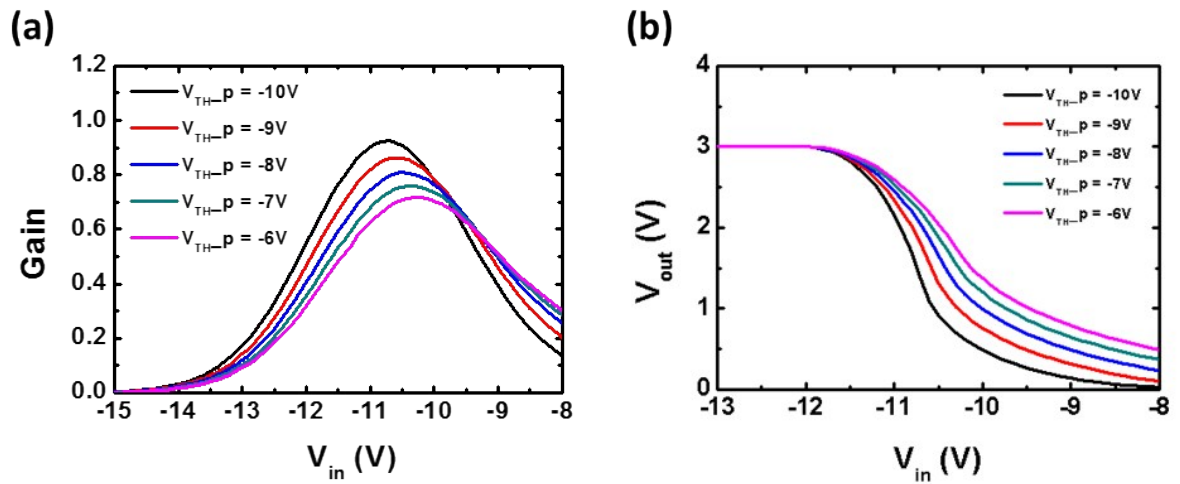


Figure S3. (a) Direct-current voltage gain and (b) voltage-transfer characteristics of CMOS inverter by SPICE simulation at $V_{dd} = 3.0$ V and different threshold voltage of P-type FET.

The simulation is performed by LT SPICE, assuming that the passivated NMOS maintains its performance and the PMOS without passivation is p-doped when exposed to NO_2 . The amount of p-doping of the exposed PMOS is changed according to the concentration of NO_2 , resulting in the right shift of the voltage gain and transfer curve.

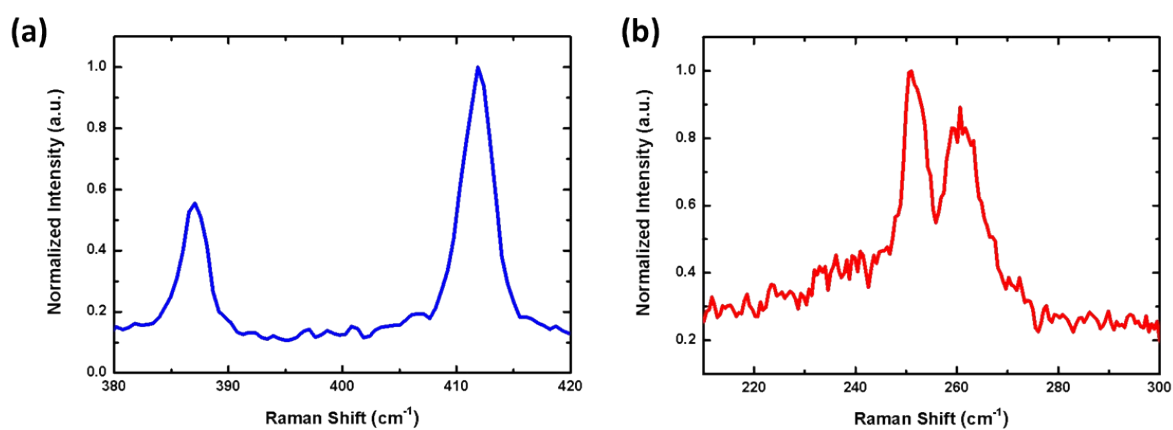


Figure S4. Normalized Raman spectra of (a) MoS₂ and (b) WSe₂.

The Raman spectroscopy performed on the MoS₂ (see Figure S4 (a)) and WSe₂ (see Figure S4 (b)) in the channel region of FETs on Al₂O₃/ITO/PET. The peak positions of the out-of-plane A_{1g} and the in-plane E_{2g}¹ peaks are at 411 cm⁻¹ and 387 cm⁻¹ in MoS₂, and 260 cm⁻¹ and 251 cm⁻¹ in WSe₂.

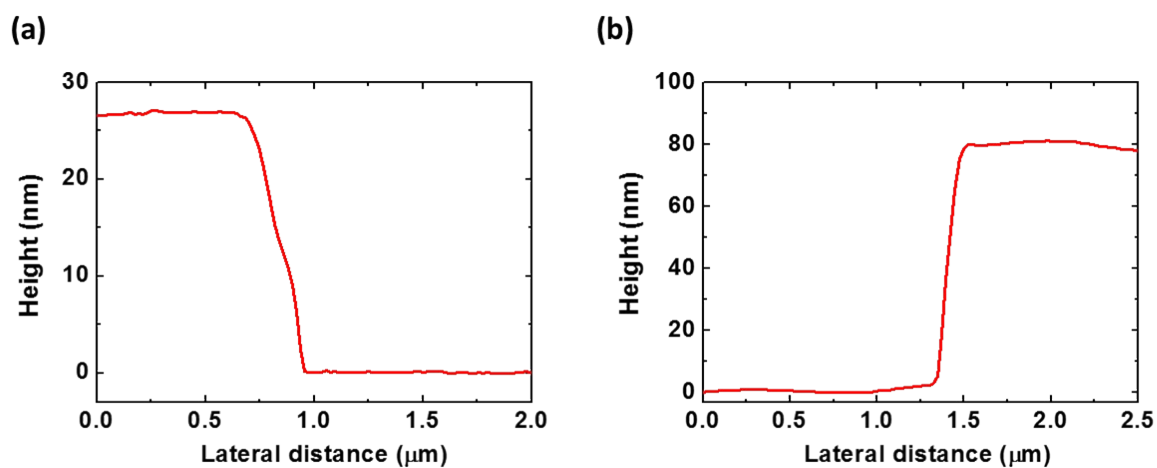


Figure S5. The thickness profile of (a) MoS₂ and (b) WSe₂.

The thickness of the MoS₂ and WSe₂ are measured by AFM, and both flakes are estimated to be 27 nm and 80 nm in thickness.

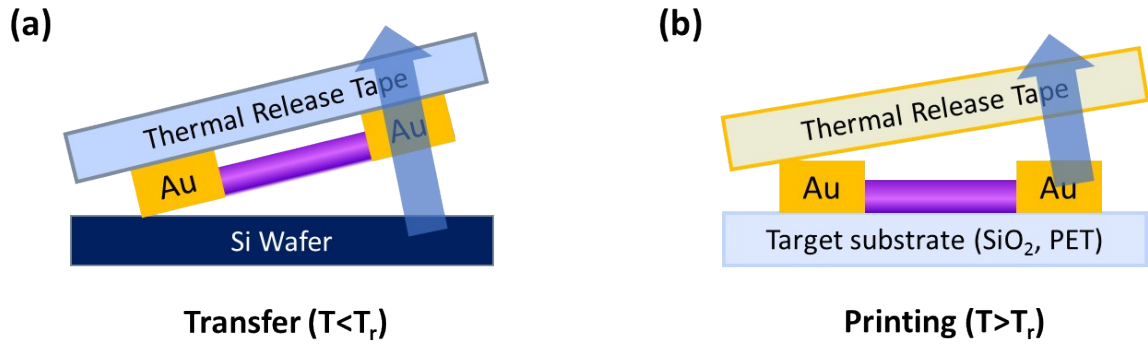


Figure S6. (a) Schematic diagram of transfer and printing using a thermal release tape.

The quantitative dependence of the energy release rate at the 2D flake/thermal release tape (TRT) interface is characterized by Equation (1) :

$$G_{TRT/flake}(v, T) = \begin{cases} \left[-e^{\gamma(T-T_r) + \ln(G_0 - G_r)} + G_0 \right] \left[1 + \left(\frac{v}{v_0} \right)^n \right] & T \leq T_r \\ G_0 \left[1 + \left(\frac{v}{v_0} \right)^n \right] & T > T_r \end{cases} \quad (1)$$

Where G_0 is the critical energy release rate when the peeling velocity approaches zero, v_0 is the reference peeling velocity at which the critical energy release rate equals to $2G_0$, and the exponent, n , is a scaling parameter that can be obtained by the experiment. T is the temperature, e is the Euler's constant, G_r is the critical energy release rate when the adhesives on TRT are deactivated, T_r is the transition temperature, γ is a material parameter.

The control of the critical energy release rate at the TRT/flake interface is mainly controlled by the peeling velocity and temperature. Therefore, we can modulate the transfer and printing of TRT by controlling temperature.